Comparison of pharmacokinetics and biodistribution of laser-synthesized plasmonic Au and TiN nanoparticles

Anton A Popov, Ivan V Zelepukin, Gleb V Tikhonowski, Elena A Popova-Kuznecova, Gleb I Tselikov, Ahmed Al-Kattan, Anne-Laure Bailly, Florian Correard, Diane Braguer, Marie-Anne Esteve, et al.

Comparison of pharmacokinetics and biodistribution of laser-synthesized plasmonic Au and TiN nanoparticles

Comparison of pharmacokinetics and biodistribution of laser-synthesized plasmonic Au and TiN nanoparticles

Anton A Popov[1,7,https://orcid.org/0000-0001-8902-0371], Ivan V Zelepukin[1,2,https://orcid.org/0000-0003-0209-2116], Gleb V Tikhonowski[1,https://orcid.org/0000-0003-4998-1631], Elena A Popova-Kuznecova[1], Gleb I Tselikov[3,https://orcid.org/0000-0002-6664-7881], Ahmed Al-Kattan[4,https://orcid.org/0000-0003-2454-8436], Anne-Laure Bailly[5], Florian Correard[5,6], Diane Braguer[5,6], Marie-Anne Esteve[5,6,https://orcid.org/0000-0001-8178-3606], Sergey M Klimentov[1], Sergey M Deyev[1,2,https://orcid.org/0000-0002-3952-0631] and Andrei V Kabashin[1,4,https://orcid.org/0000-0003-1549-7198]

[1] MEPhI, Institute of Engineering Physics for Biomedicine (PhysBio), Moscow, 115409, Russia
[2] Shemyakin–Ovchinnikov Institute of Bioorganic Chemistry, Russian Academy of Sciences, Moscow, 117997, Russia
[3] Moscow Institute of Physics and Technology, Center for Photonics and 2D Materials, Dolgoprudny 141700, Russia
[4] Aix Marseille Univ, CNRS, LP3, Marseille, 13288, France
[5] Aix Marseille Univ, CNRS, INP, Inst Neurophysiopathol, Marseille, 13288, France
[6] APHM, Hôpital de la Timone, Service Pharmacie, Marseille, 13288, France
[7] Corresponding author: aapopov1@mephi.ru

Abstract. Plasmonic nanostructures offer wide range of diagnostic and therapeutic functionalities for biomedical applications. Gold nanoparticles (Au NPs) present one of the most explored nanomaterial in this field, while titanium nitride nanoparticles (TiN NPs) is a new promising nanomaterial with superior plasmonic properties for biomedicine. However conventional chemical techniques for the synthesis of these nanomaterials cannot always match stringent requirements for toxicity levels and surface conditioning. Laser-synthesized Au and TiN NPs offer exceptional purity (no contamination by by-products or ligands) and unusual surface chemistry. Therefore, these NPs present a viable alternative to chemically synthesized counterparts. This work presents comparative analysis of pharmacokinetics and biodistribution of laser-synthesized 20 nm Au and TiN NPs under intravenous administration in mice model. Our data show that Au NPs and bare TiN NPs are rapidly eliminated from the blood circulation and accumulate preferentially in liver and spleen, while coating of TiN NPs by hydrophilic polymer polyethylene glycol (PEG) significantly prolongates blood circulation time and improves delivery of the NPs to tumor. We finally discuss potential applications of laser synthesized Au NPs in SERS, SEIRA and electrocatalysis, while TiN nanoparticles are considered as promising agents for photothermal therapy and photoacoustic imaging.

1. Introduction

Plasmonic nanoparticles (NPs) is one of the most promising classes of nanosized inorganic materials for medical and biosensing applications [1]. These NPs exhibit a resonant absorption and scattering features in optical spectra with the corresponding cross-sections exceeding that of conventional absorbing dyes by many orders of magnitude [2]. The most prominent plasmonic-based therapeutic modality is

photothermal therapy (PTT) [3,4], which profits from a conversion of external light into heat for local destruction of cancer cells and stimulation of anti-tumor immune response of the organism [5]. The same photoheating effect gives rise to a photoacoustic imaging (PAI) modality [6,7], which can be used to visualize the tumor area.

Gold nanoparticles (Au NPs) is one of the most explored plasmonic nanomaterial for biomedical applications due to chemical stability and good biocompatibility of gold. Au NPs has already been used in several diagnostic and therapeutic modalities, including PTT [8], confocal reflectance microscopy [9], photoacoustic tomography [10] and optical coherence tomography [11].

Titanium nitride nanoparticles (TiN NPs) is an alternative plasmonic nanomaterial for biomedical applications [12–14]. One of the most prominent advantages of this material is its plasmonic feature located right in the biological tissue transparency window around 650–800 nm. The feasibility of using TiN NPs as contrast agents in PAI and as sensitizers of PTT for cancer curing has already been confirmed [15].

Both of these nanomaterials are very promising candidates for plasmonic-based *in vivo* applications in nanomedicine. However, this field is very demanding to properties of the nanomaterials. The requirements include uniform size and shape, high biocompatibility, low visibility to the immune system, biodegradability or clearance from an organism [1]. Such requirements are hardly satisfied by conventional synthesis pathways. Indeed, methods of colloidal chemistry e.g., reverse micelles or the reduction of a metal precursor in the presence of capping agents [16,17] typically cause surface contamination by residual by-products and ligands, which can cause toxicity issues [18]. Moreover, Au NPs with non-spherical geometry (nanorods, nanocages, nanostars, etc.) which have biologically relevant plasmonic feature typically requires special surfactants and protecting ligands that can lead to severe toxicity effects. As an example, synthesis of Au nanorods require the use of cetyl trimethylammonium bromide (CTAB), which causes high toxicity of Au nanorods colloids [19]. On the other hand, alternative dry methods, which can be used for fabrication of TiN NPs (e.g., a direct nitridation of TiO_2 powders [20] or plasma assisted processing [21]) typically result in widely size-dispersed nanostructures of irregular shape in partially aggregated state [15,21], which complicates their stabilization in colloidal solutions, delivery *in vivo* and clearance from the body. Thus, the problem of efficient synthesis of pure uncontaminated colloids of plasmonic NPs is still actual.

We recently reported the synthesis of different types of extremely clean (free of residual contamination) colloidal NPs including plasmonic Au and TiN NPs by facile physical methods of femtosecond (fs) pulsed laser ablation in liquids (PLAL) [14,22–26]. We demonstrated that this method enables control of mean size of the synthesized NPs under relatively narrow size dispersion. Laser-synthesized NPs typically demonstrate excellent colloidal stability in absence of any stabilizing agents due to a strong negative charge of NPs leading to the electrostatic repulsion effect [27]. Moreover, our approach allows one to synthesize NPs with complex composition and geometry [28,29]. Both laser synthesized Au and TiN NPs types were thoroughly evaluated *in vivo* and *in vitro* [30-32]. The results demonstrate their good biocompatibility and favorable pharmacokinetics, which makes them very promising for the aforementioned biomedical applications.

Here, we present comparative analysis of pharmacokinetics and biodistribution of small (20-30 nm) plasmonic Au and TiN NPs in mouse model. We demonstrate that both types of NPs have similar blood circulation time, while coverage of TiN NPs by hydrophilic biopolymer polyethylene glycol (PEG) significantly prolongs that time and increase accumulation of PEG coated NPs in tumor. Both NPs preferentially accumulate in liver and spleen, but distribution among the other organs is different for Au and TiN NPs. The results confirm that covering of NPs by a hydrophilic polymers after the laser synthesis leads to prolongation of their blood circulation time and increase of their tumor accumulation.

2. Experimental methods

The NPs were synthesized by fs PLAL at ambient conditions, as described in details in our previous papers [14,30,32-34]. Au NPs we prepared using a Yb:KGW laser (1025 nm, 480 fs, 100 μJ per pulse, 10 kHz repetition rate). The laser beam was focused by 75 mm lens onto the surface of Au target

(99.99%, GoodFellow, France) placed on the bottom of a glass vessel filled with 1 cm layer of deionized water containing 1 mg/mL of dextran (MW ~40,000, Sigma-Aldrich), which was used to achieve better size control of the Au NPs and to cover them with hydrophilic polymeric coating. The ablation target was moved horizontally at 0.5 mm/s speed during the experiment. For the synthesis of TiN NPs, a TiN target was fixed vertically on the wall of a glass vessel filled with 14 mL of analytical grade acetone. Radiation from a Yb:KGW laser (1030 nm, 270 fs, 50 μJ per pulse, 10 kHz repetition rate) was focused by a 75 mm lens on the surface of the target through a side wall of the vessel. The thickness of the liquid layer from the entrance glass to the target surface was 7 mm. The ablation vessel was moved at 5 mm/s speed. A minor fraction of relatively large (~100 nm) TiN NPs were removed by centrifugation at 1000 g for 15 min. Half of the TiN NPs were covered with PEG molecules using modified Stober method. For this, 1 mg of TiN NPs was transferred to 1 mL of 96% ethanol, then 65 mL of distilled water and 20 mL of 30% ammonia hydroxide were added. Then the dispersion was ultrasonicated, and 100 mL of 1 g/L mPEG-Silane solution in ethanol was quickly dropped to it under stirring. After that, the dispersion was heated to 60 °C for 2 h followed by incubation at room temperature overnight. Finally, the PEG coated TiN NPs (TiN-PEG NPs) were separated by washing the dispersion 3 times with ethanol and one time with distilled water.

Morphology and size of the synthesized NPs were characterized by means of the high-resolution transmission electron microscopy (HR-TEM) system (JEOL JEM 3010), operating at 300 kV. Samples were prepared by dropping 5 μL of NPs solution onto a carbon-coated copper grid and subsequent drying at ambient conditions. Qualitative chemical composition was measured by an energy-dispersive spectroscopy (EDS) detector (X-act, Oxford Instruments, High Wycombe, UK) coupled with scanning electron microscope (MAIA 3, Tescan, Czech Republic) operating at 15 kV. Samples for the EDS measurements were fixed on a silicon substrate.

All experimental protocols and animal analyses for determination of pharmacokinetics and biodistribution assessment of Au NPs were conducted in accordance with the guidelines of the French Government and the Regional Committee for Ethics on Animal Experiments (authorization number 0100903). The experimental procedure was approved by the Committee for Ethics on Animal Experiments of the Institute of NeuroPhysiopathology. In the experiments with Au NPs six weeks old athymic nude female mice (Harlan, France) were used. For the pharmacokinetic study of Au NPs mice were administered intravenously with the 1 mg/kg of Au NPs. Animals were sacrificed at: 5 min, 15 min, 30 min, 45 min, 60 min and 4 h after the NPs injection and blood samples (800 μL) were collected by intra-cardiac puncture. Before the biodistribution tests human glioblastoma cells (U87-MG, $2.5x10^6$) were administered subcutaneously to all mice. When the tumor reached approximately 100 mm^3, mice were intravenously administered with a single dose of 1 mg/kg Au NPs diluted in phosphate buffer saline (PBS). At the same time, control group of mice were injected with pure PBS without NPs. Animals were sacrificed at 24 h post injection. The liver, spleen, kidneys, lungs, heart, brain, tumor were removed to measure Au content. The obtained samples were mineralized followed by dilution with water and analyzed by inductively coupled mass spectrometry (ICP-MS).

All animal studies with TiN NPs were carried out in strict accordance with the provisions of the European Convention for the Protection of Vertebrate Animals Used for Experimental and Other Scientific Purposes and was approved by the Institutional Animal Care and Use Committee of Shemyakin–Ovchinnikov Institute of Bioorganic Chemistry (Moscow, Russia). Female BALB/c mice were used in the experiments. Animals bearing 300 ± 100 mm^3 mammary EMT6/P tumor were used. Blood samples for pharmacokinetic analysis were taken from the opposite retroorbital sinus. For the pharmacokinetic study of TiN NPs 200 μg of TiN NPs were injected intravenously, then 20 μL of blood was taken at 1, 5, 15, 30, 60, 120 and 180 min after the NPs injection. For biodistribution tests, mice were euthanized 180 min after TiN NPs injection. Then organs were extracted and weighted. All the samples were mineralized followed by dilution with water and measured by ICP-MS.

3. Results and discussion

Plasmonic Au and TiN NPs were synthesized by fs PLAL as described in Experimental methods section. Fabrication of Au NPs was performed in aqueous solutions of dextran polymer in order to obtain the NPs with desirable size (20-30 nm) in one step and at the same time to cover them with a polymer to increase colloidal stability in biologically relevant liquids. The possibility of *in situ* coating of the NPs during synthesis in one of the unique features of PLAL. The methodology of preparation of TiN NPs was different. The TiN NPs were originally synthesized by fs PLAL in acetone to reduce their oxidation, which negatively affects plasmonic properties of TiN NPs. Then the NPs were transferred to water and half of them were further coated with hydrophilic polymer PEG. The PEG coating was done in order to improve colloidal stability of the NPs in the bloodstream and to decrease the rate of NPs elimination by the immune system. Both of these parameters affect successful delivery of NPs to solid tumors [35]. Therefore, the PEG coating was ultimately intended to increase the accumulation of the NPs in the tumor. In total we had three NPs samples for testing their pharmacokinetics and biodistribution, namely Au NPs with dextran coating, bare TiN NPs and TiN-PEG NPs.

Physicochemical characterization of the NPs is demonstrated in figure 1.

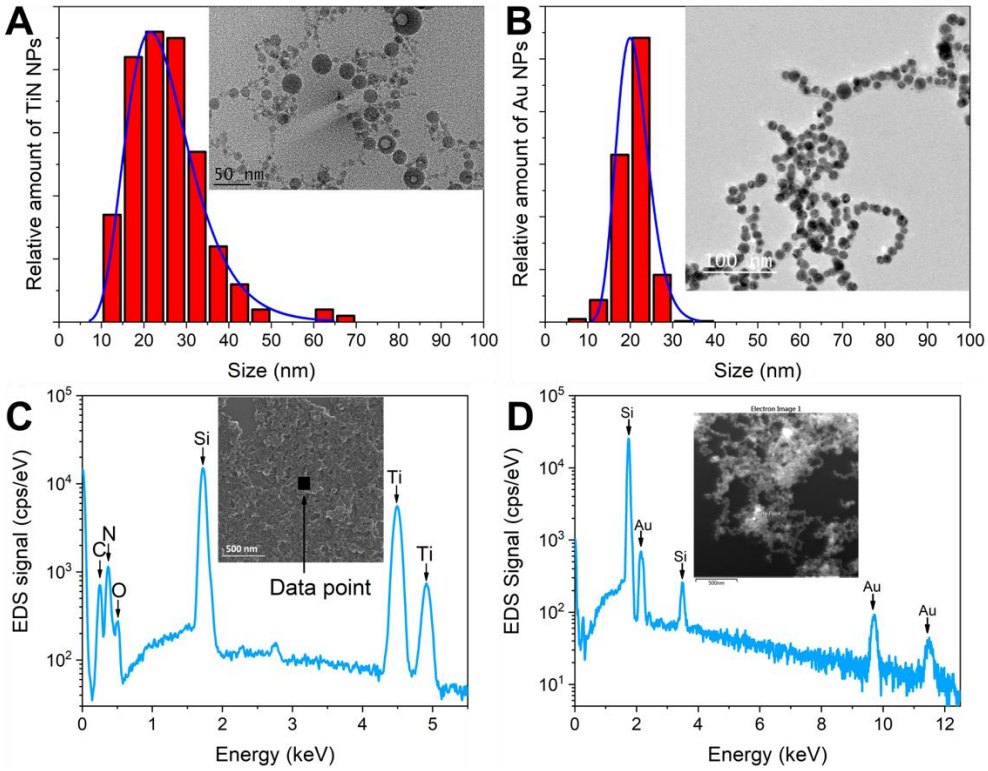

Figure 1. Physicochemical characterization of NPs. (A, B) Size distributions of TiN and Au NPs correspondingly. Insets demonstrate typical TEM images of the NPs. (C, D) Qualitative chemical composition of TiN and Au NPs correspondingly measured by EDS technique. Insets demonstrate points of spectral data collection.

Typical TEM images of TiN and Au NPs are shown in insets to figure 1A and 1B correspondingly. Morphology of both types of NPs was predominantly spherical. Statistical analysis of TEM images revealed lognormal number-weighted distributions of NPs sizes with similar mode values (19.2 nm for Au NPs and 21.5 nm for TiN NPs). This size of NPs is favorable for biomedical applications because it is small enough for effective activation of passive tumor accumulation mechanism based on EPR effect [36], but at the same time this size range is larger than glomerular filtration cut-off size and therefore

the NPs are not rapidly cleared from the blood circulation via renal filtration [37]. Note also that width of size distribution was much narrower for Au NPs than for TiN NPs (standard deviations are 3.9 and 8.9 nm correspondingly). This difference is explained by the presence of dextran in ablation liquid during synthesis of Au NPs. In our previous works we demonstrated that addition of various polymers into ablation medium can reduce mean size of NPs and narrow down their size distribution [32]. Therefore, both TiN and Au NPs had equal sizes and morphology and these parameters should equally affect biodistribution and pharmacokinetics of the NPs. EDS data demonstrated in figure 1C and 1D confirm qualitative chemical composition of the NPs. Here, in TiN NP sample the main signals in the spectrum corresponded to nitrogen (N) and titanium (Ti), while small oxygen (O) and carbon (C) signals are related to residual oxidation of the NPs and to products of acetone drying. In Au NPs only signals from Au are present, which confirm their high purity. Presence of silicon (Si) peak in spectra of both samples originated from the Si substrate.

The *in vivo* tests were performed using murine models. Tumor bearing mice were injected with NPs and pharmacokinetics along with biodistribution were studied using ICP-MS. NPs concentrations in the bloodstream were determined between 5 min and 4 h for Au NPs and between 1 min and 3 h for TiN and TiN-PEG NPs after intravenous injection of NPs. As shown in figure 2A, bare TiN NPs and Au NPs had similar pharmacokinetic profile with a short half-life time in the bloodstream and were rapidly cleared. In particular, after just 5 min after the injection we observed only 6.8% ID of TiN NPs and 1.1% ID of Au NPs in the bloodstream. However, TiN-PEG NPs had significantly improved circulation time. Five min after the NPs administration there were still more than 50% ID of TiN-PEG NPs in the bloodstream, moreover TiN-PEG NPs were detectable at substantial level even 1 h after the administration.

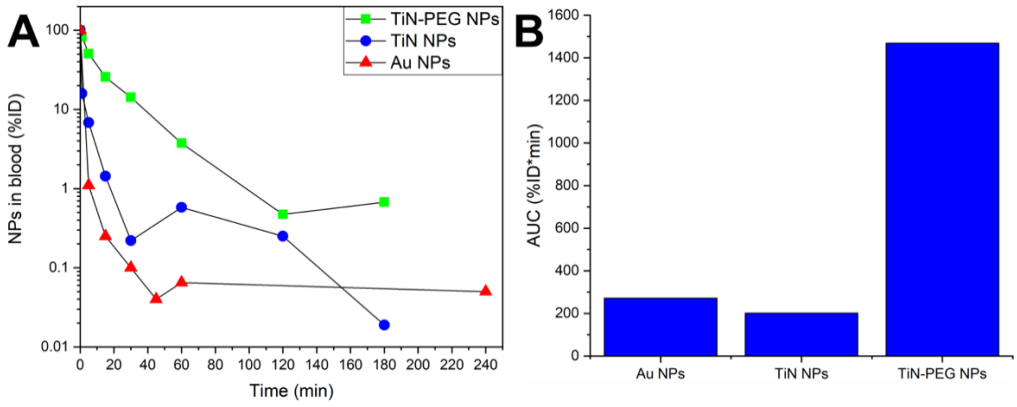

Figure 2. Pharmacokinetics data of Au, TiN and TiN-PEG NPs. (A) Blood circulation kinetics measured by ICP-MS. (B) AUC of circulation kinetics during the first 3 h after the NPs administration.

The obtained curves cannot be fitted by an exponential function due to complex pharmacokinetic behavior. Therefore, to quantitatively compare the circulation kinetics of all NPs types, we used area under the curve (AUC) parameter for the first 3 hours after the NPs injection. This parameter is commonly used in similar cases. The results are shown in figure 2B. As one can see from the data, Au and bare TiN NPs had similar AUC, while the relative parameter for TiN-PEG NPs was more than 7-fold higher. This dramatic prolongation of TiN-PEG NPs circulation can be explained by “stealth” properties of PEG polymer.

The biodistribution of all NPs was studied using data from tumor and all the major organs: liver, spleen, lungs, kidneys, heart, brain. The data were collected after all the administrated NPs were removed from the bloodstream. Results of the biodistribution analysis normalized to the maximum observed concentrations are presented in figure 3.

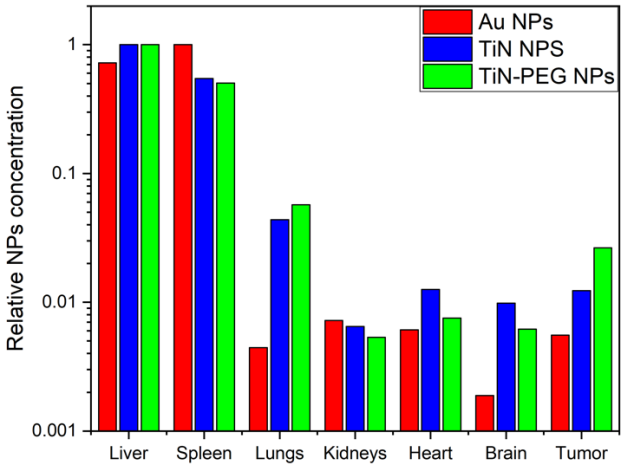

Figure 3. Biodistribution of Au, TiN and TiN-PEG NPs in organs of mice (n=3).

Direct comparison of the absolute amounts of NPs was not possible because different doses of Au and TiN-based NPs were administrated to mice. All types of NPs were predominantly accumulated in liver and spleen, however concentrations per gram of the tissue of both TiN and TiN-PEG NPs were the highest in liver, where concentration of Au NPs consisted only 72% of that in spleen. While Au NPs had the highest concentration per gram of the tissue in spleen, where TiN and TiN-PEG NPs had 55% and 50% correspondingly of their concentrations in liver. Note also that there was significantly lower relative concentration of Au NPs in lungs compared to both TiN and TiN-PEG NPs. This result can be due to presence of relatively large TiN NPs, which can get stuck in the smallest capillary in lungs. Indeed, according to figure 1A and 1B there were almost no Au NPs with sizes large than 30 nm, while substantial fraction of TiN NPs had sizes above 30 nm. Another observation that can be explained by minor size differences between NPs is slightly higher accumulation of Au NPs in kidneys. This result can be due to presence of Au NPs with sizes less than 10 nm, which are typically removed from an organism through kidney, therefore presence of smallest Au NPs leads to their higher accumulation in that organ. Finally, there was a significant difference between tumor accumulation of the NPs. TiN-PEG NPs had more than 5-fold better tumor accumulation if compared with Au NPs and more 2-fold increased tumor accumulation if compared with bare TiN NPs. This result can be due to increased blood circulation time of TiN-PEG NPs compared to other tested types of NPs. This prolongation of the blood circulation made possible their efficient delivery to tumor and accumulation via enhanced permeability and retention (EPR) effect [36]. We should note that the aforementioned differences can also be caused by the different time elapsed after the injection of NPs until the biodistribution measurements: concentrations of Au NPs were measured 24 h after the injection, while TiN and TiN-PEG NPs 3 h after the injection.

The presented data can be used for rational design of further works with plasmonic laser synthesized NPs. As an example, laser synthesized Au NPs can be of interest for a wide range of biomedical applications. These NPs can be an efficient probe for field-enhanced spectroscopies e.g., surface enhanced Raman scattering (SERS) or surface enhanced IR absorption (SEIRA). Superiority of laser synthesized Au NPs with “bare” surface for SERS has several reasons. First, exempt of ligands or contaminants eliminates parasitic background noises originated from NPs surface. Second, quenching of autofluorescence of target biomolecules from direct contact between bare surface of laser synthesized Au NPs and the biomolecules due to Foerster resonance energy transfer (FRET) effect. The advantages were demonstrated in our recent comparative tests involving laser-synthesized Au NPs and different chemical counterparts as SERS probes for the identification of beverage spoilage yeasts [38]. We found that bare laser-synthesized NPs outperform all counterparts in terms of signal-to-noise ratio. As an alternative example, we used Au-based NPs as probes for the identification of Listeria innocua and

Escherichia coli bacteria by SERS [39]. We also believe that these Au NPs can be used as promising building blocks and tags in plasmonic biosensors [40–43].

It is worth to note that the described results continue a cycle of studies devoted to the assessment of novel nanomaterials prepared by "green" laser-ablative synthesis for biomedical applications. In previous studies [44–46] we examined laser-synthesized silicon (Si) NPs which possess a series of unique imaging [47] and therapeutic [48] features. Our tests demonstrated that Si NPs are safe and biodegradable so that they can rapidly decay into orthosilicic acid and excrete from an organism with the urine within several days [46]. In contrast to widely explored Au- and Si-based NPs, which already gained substantial attention in the field of biomedical applications, TiN NPs is a new material with superior photothermal characteristics compared to other plasmonic counterparts. Although TiN NPs weakly enhance electromagnetic fields, and therefore are hardly useful in SERS, these NPs have their plasmonic peak in the window of relative tissue transparency (650-800 nm), which makes them a good candidate for PTT and PAI. We demonstrated high biocompatibility of TiN NPs and found a strong photothermal effect by using TiN NPs as sensitizers of IR PTT. Altogether, our results demonstrate that laser synthesized Au and TiN NPs are very promising for both *in vitro* and *in vivo* biomedical applications.

4. Conclusions

Biodistribution and pharmacokinetics of ultrapure fs PLAL-synthesized Au, TiN and TiN-PEG NPs with sizes in the range of 20-30 nm were measured in murine mice model. It is shown that Au and bare TiN NPs are rapidly eliminated from the bloodstream, while coating of TiN NPs with PEG increases circulation time of NPs in the bloodstream and enhance efficiency of their passive delivery to tumor target. In particular, TiN-PEG NPs had 7-fold higher AUC of their pharmacokinetic curve during first 3 h after NPs administration compared to both Au and bare TiN NPs. After systemic administration all NPs were mainly accumulated in liver and spleen, while TiN-based NPs were more concentrated in liver and Au NPs in spleen. Finally TiN-PEG NPs had 5-fold and 2-fold better accumulation in tumor than Au and TiN NPs accordingly. The presented results make laser-synthesized Au and TiN NPs very attractive for the development of novel therapeutic and imaging modalities profiting from their superior plasmonic properties.

Acknowledgements

The authors acknowledge financial support of the Russian Science Foundation (Project 19-72-30012) for synthesis of nanomaterials and in vivo tests of TiN and TiN-PEG NPs. The authors also acknowledge the support from the Ministry of Education and Science of the Russian Federation (Project FSWU-2020-0035) for providing the research equipment and the related scientific infrastructure.

References

[1] Prasad P N 2012 *Introduction to nanomedicine and nanobioengineering* (New Jersey: John Wiley & Sons, Inc.)
[2] Jain P K, Lee K S, El-Sayed I H and El-Sayed M A 2006 Calculated absorption and scattering properties of gold nanoparticles of different size, shape, and composition: applications in biological imaging and biomedicine *J. Phys. Chem. B* **110** 7238–48
[3] Jain P K, Huang X, El-Sayed I H and El-Sayed M A 2008 Noble Metals on the Nanoscale: Optical and Photothermal Properties and Some Applications in Imaging, Sensing, Biology, and Medicine *Acc. Chem. Res.* **41** 1578–86
[4] Rastinehad A R, Anastos H, Wajswol E, Winoker J S, Sfakianos J P, Doppalapudi S K, Carrick M R, Knauer C J, Taouli B, Lewis S C, et al 2019 Gold nanoshell-localized photothermal ablation of prostate tumors in a clinical pilot device study *Proc. Natl. Acad. Sci.* **116** 18590–6
[5] Toraya-Brown S and Fiering S 2014 Local tumour hyperthermia as immunotherapy for metastatic cancer *Int. J. Hyperth.* **30** 531–9
[6] Gargiulo S, Albanese S and Mancini M 2019 State-of-the-Art Preclinical Photoacoustic

Imaging in Oncology: Recent Advances in Cancer Theranostics *Contrast Media Mol. Imaging* **2019** 1–24
[7] Maldonado M E, Das A, Gomes A S L, Popov A A, Klimentov S M and Kabashin A V. 2020 Nonlinear photoacoustic response of suspensions of laser-synthesized plasmonic titanium nitride nanoparticles *Opt. Lett.* **45** 6695
[8] Huang X, El-Sayed I H, Qian W and El-Sayed M A 2006 Cancer cell imaging and photothermal therapy in the near-infrared region by using gold nanorods *J. Am. Chem. Soc.* **128** 2115–20
[9] Sokolov K, Follen M, Aaron J, Pavlova I, Malpica A, Lotan R and Richards-Kortum R 2003 Real-time vital optical imaging of precancer using anti-epidermal growth factor receptor antibodies conjugated to gold nanoparticles *Cancer Res.* **63** 1999–2004
[10] Gobin A M, Lee M H, Halas N J, James W D, Drezek R A and West J L 2007 Near-infrared resonant nanoshells for combined optical imaging and photothermal cancer therapy *Nano Lett.* **7** 1929–34
[11] Nguyen V P, Qian W, Li Y, Liu B, Aaberg M, Henry J, Zhang W, Wang X and Paulus Y M 2021 Chain-like gold nanoparticle clusters for multimodal photoacoustic microscopy and optical coherence tomography enhanced molecular imaging *Nat. Commun.* **12** 34
[12] Wang C, Dai C, Hu Z, Li H, Yu L, Lin H, Bai J and Chen Y 2019 Photonic cancer nanomedicine using the near infrared-II biowindow enabled by biocompatible titanium nitride nanoplatforms *Nanoscale Horizons* **4** 415–25
[13] Boltasseva A and Shalaev V M 2015 All that glitters need not be gold *Science (80-.).* **347** 1308–10
[14] Popov A A, Tselikov G, Dumas N, Berard C, Metwally K, Jones N, Al-Kattan A, Larrat B, Braguer D, Mensah S, et al 2019 Laser- synthesized TiN nanoparticles as promising plasmonic alternative for biomedical applications *Sci. Rep.* **9** 1194
[15] He W, Ai K, Jiang C, Li Y, Song X and Lu L 2017 Plasmonic titanium nitride nanoparticles for in vivo photoacoustic tomography imaging and photothermal cancer therapy *Biomaterials* **132** 37–47
[16] Kimling J, Maier M, Okenve B, Kotaidis V, Ballot H and Plech A 2006 Turkevich Method for Gold Nanoparticle Synthesis Revisited *J. Phys. Chem. B* **110** 15700–7
[17] Gole A and Murphy C J 2004 Seed-Mediated Synthesis of Gold Nanorods: Role of the Size and Nature of the Seed *Chem. Mater.* **16** 3633–40
[18] Gerber A, Bundschuh M, Klingelhofer D and Groneberg D A 2013 Gold nanoparticles: recent aspects for human toxicology *J. Occup. Med. Toxicol.* **8** 32
[19] Fratoddi I, Venditti I, Cametti C and Russo M V 2015 How toxic are gold nanoparticles? The state-of-the-art *Nano Res.* **8** 1771–99
[20] Li J, Gao L, Sun J, Zhang Q, Guo J and Yan D 2001 Synthesis of nanocrystalline titanium nitride powders by direct nitridation of titanium oxide *J. Am. Ceram. Soc.* **84** 3045–7
[21] Tavares J, Coulombe S and Meunier J-L 2009 Synthesis of cubic-structured monocrystalline titanium nitride nanoparticles by means of a dual plasma process *J. Phys. D. Appl. Phys.* **42** 102001
[22] Maximova K, Aristov A, Sentis M and Kabashin A V 2015 Size-controllable synthesis of bare gold nanoparticles by femtosecond laser fragmentation in water *Nanotechnology* **26** 065601
[23] Al-Kattan A, Nirwan V, Popov A, Ryabchikov Y, Tselikov G, Sentis M, Fahmi A and Kabashin A 2018 Recent Advances in Laser-Ablative Synthesis of Bare Au and Si Nanoparticles and Assessment of Their Prospects for Tissue Engineering Applications *Int. J. Mol. Sci.* **19** 1563
[24] Lim C-K, Popov A A, Tselikov G, Heo J, Pliss A, Kim S, Kabashin A V. and Prasad P N 2018 Organic Solvent and Surfactant Free Fluorescent Organic Nanoparticles by Laser Ablation of Aggregation-Induced Enhanced Emission Dyes *Adv. Opt. Mater.* **1800164** 1800164
[25] Bulmahn J C, Tikhonowski G, Popov A A, Kuzmin A, Klimentov S M, Kabashin A V. and

Prasad P N 2020 Laser-Ablative Synthesis of Stable Aqueous Solutions of Elemental Bismuth Nanoparticles for Multimodal Theranostic Applications *Nanomaterials* **10** 1463

[26] Popova-Kuznetsova E, Tikhonowski G, Popov A A, Duflot V, Deyev S, Klimentov S, Zavestovskaya I, Prasad P N and Kabashin A V 2019 Laser-Ablative Synthesis of Isotope-Enriched Samarium Oxide Nanoparticles for Nuclear Nanomedicine *Nanomaterials* **10** 69

[27] Sylvestre J P, Poulin S, Kabashin A V, Sacher E, Meunier M and Luong J H T 2004 Surface chemistry of gold nanoparticles produced by laser ablation in aqueous media *J. Phys. Chem. B* **108** 16864–9

[28] Ryabchikov Y, Popov A A, Sentis M, Timoshenko V Y and Kabashin A V. 2016 Structural properties of gold-silicon nanohybrids formed by femtosecond laser ablation in water at different fluences *Synthesis and Photonics of Nanoscale Materials XIII* vol 9737, ed A V. Kabashin, D B Geohegan and J J Dubowski (San-Francisko) p 97370F

[29] Al-Kattan A, Tselikov G, Metwally K, Popov A A, Mensah S and Kabashin A V 2021 Laser Ablation-Assisted Synthesis of Plasmonic Si@Au Core-Satellite Nanocomposites for Biomedical Applications *Nanomaterials* **11** 592

[30] Bailly A, Correard F, Popov A, Tselikov G, Chaspoul F, Appay R, Al-Kattan A, Kabashin A V, Braguer D and Esteve M-A 2019 In vivo evaluation of safety, biodistribution and pharmacokinetics of laser-synthesized gold nanoparticles *Sci. Rep.* **9** 12890

[31] Zelepukin I V., Popov A A, Shipunova V O, Tikhonowski G V., Mirkasymov A B, Popova-Kuznetsova E A, Klimentov S M, Kabashin A V. and Deyev S M 2021 Laser-synthesized TiN nanoparticles for biomedical applications: Evaluation of safety, biodistribution and pharmacokinetics *Mater. Sci. Eng. C* **120** 111717

[32] Correard F, Maximova K, Estève M-A, Villard C, Roy M, Al-Kattan A, Sentis M, Gingras M, Kabashin A V and Braguer D 2014 Gold nanoparticles prepared by laser ablation in aqueous biocompatible solutions: assessment of safety and biological identity for nanomedicine applications. Int. J. Nanomedicine 9 5415–30

[33] Kabashin A V, Meunier M, Kingston C and Luong J H T 2003 Fabrication and Characterization of Gold Nanoparticles by Femtosecond Laser Ablation in an Aqueous Solution of Cyclodextrins *J. Phys. Chem. B* **107** 4527–31

[34] Besner S, Kabashin A V., Winnik F M and Meunier M 2009 Synthesis of size-tunable polymer-protected gold nanoparticles by femtosecond laser-based ablation and seed growth *J. Phys. Chem. C* **113** 9526–31

[35] Suk J S, Xu Q, Kim N, Hanes J and Ensign L M 2016 PEGylation as a strategy for improving nanoparticle-based drug and gene delivery *Adv. Drug Deliv. Rev.* **99** 28–51

[36] Torchilin V 2011 Tumor delivery of macromolecular drugs based on the EPR effect *Adv. Drug Deliv. Rev.* **63** 131–5

[37] Yu M and Zheng J 2015 Clearance Pathways and Tumor Targeting of Imaging Nanoparticles *ACS Nano* **9** 6655–74

[38] Uusitalo S, Popov A, Ryabchikov Y V., Bibikova O, Alakomi H L, Juvonen R, Kontturi V, Siitonen S, Kabashin A, Meglinski I, et al 2017 Surface-enhanced Raman spectroscopy for identification and discrimination of beverage spoilage yeasts using patterned substrates and gold nanoparticles *J. Food Eng.* **212** 47–54

[39] Kögler M, Ryabchikov Y V., Uusitalo S, Popov A, Popov A, Tselikov G, Välimaa A-L, Al-Kattan A, Hiltunen J, Laitinen R, et al 2018 Bare laser-synthesized Au-based nanoparticles as nondisturbing surface-enhanced Raman scattering probes for bacteria identification *J. Biophotonics* **11** e201700225

[40] Anker J N, Hall W P, Lyandres O, Shah N C, Zhao J and Van Duyne R P 2009 Biosensing with plasmonic nanosensors *Nanoscience and Technology* vol 7 (Co-Published with Macmillan Publishers Ltd, UK) pp 308–19

[41] Aristov A I, Manousidaki M, Danilov A, Terzaki K, Fotakis C, Farsari M and Kabashin A V. 2016 3D plasmonic crystal metamaterials for ultra-sensitive biosensing *Sci. Rep.* **6** 25380

[42] Kabashin A V, Kochergin V E and Nikitin P I 1999 Surface plasmon resonance bio- and chemical sensors with phase-polarisation contrast *Sensors Actuators B Chem.* **54** 51–6
[43] Patskovsky S, Kabashin A V., Meunier M and Luong J H T 2003 Silicon-based surface plasmon resonance sensing with two surface plasmon polariton modes *Appl. Opt.* **42** 6905
[44] Petriev V M, Tischenko V K, Mikhailovskaya A A, Popov A A, Tselikov G, Zelepukin I, Deyev S M, Kaprin A D, Ivanov S, Timoshenko V Y, et al 2019 Nuclear nanomedicine using Si nanoparticles as safe and effective carriers of 188Re radionuclide for cancer therapy *Sci. Rep.* **9** 2017
[45] Al-Kattan A, Ryabchikov Y V, Baati T, Chirvony V, Sánchez-Royo J F, Sentis M, Braguer D, Timoshenko V Y, Estève M-A and Kabashin A V 2016 Ultrapure laser-synthesized Si nanoparticles with variable oxidation states for biomedical applications *J. Mater. Chem. B* **4** 7852–8
[46] Baati T, Al-Kattan A, Esteve M-A, Njim L, Ryabchikov Y, Chaspoul F, Hammami M, Sentis M, Kabashin A V. and Braguer D 2016 Ultrapure laser-synthesized Si-based nanomaterials for biomedical applications: in vivo assessment of safety and biodistribution *Sci. Rep.* **6** 25400
[47] Kharin A Y, Lysenko V V., Rogov A, Ryabchikov Y V., Geloen A, Tishchenko I, Marty O, Sennikov P G, Kornev R A, Zavestovskaya I N, et al 2019 Bi-Modal Nonlinear Optical Contrast from Si Nanoparticles for Cancer Theranostics *Adv. Opt. Mater.* **7** 1801728
[48] Oleshchenko V A, Yu. Kharin A, Alykova A F, Karpukhina O V, Karpov N V, Popov A A, Bezotosnyi V V, Klimentov S M, Zavestovskaya I N, Kabashin A V, et al 2020 Localized infrared radiation-induced hyperthermia sensitized by laser-ablated silicon nanoparticles for phototherapy applications *Appl. Surf. Sci.* **516** 145661